Dynamic Strain Measurement Using Small Gain Stimulated Brillouin Scattering in STFT-BOTDR

Bo Li, Linqing Luo, Yifei Yu, Kenichi Soga, and Jize Yan

Abstract—A distributed dynamic strain measurement is demonstrated using small gain stimulated Brillouin scattering (SBS) in Brillouin optical time domain reflectometry based on the short-time Fourier transform algorithm. The input power limits, frequency uncertainties for given pulse durations, fiber lengths, and the number of averaging are calculated. The output signal power and the signal-to-noise ratio of the system output are enhanced by SBS. It is found that the signal processing is faster and requires fewer averaging to achieve dynamic sensing performance along the fiber under test. A 60-Hz vibration on a 6-m fiber section at the end of a 935-m fiber is detected with the spatial resolution of 4 m with a sampling rate of 2.5 kS/s.

Index Terms—Brillouin scattering, distributed fiber optic sensors, strain measurement.

I. INTRODUCTION

IN RECENT years, structural health monitoring (SHM) is becoming critical in structural and geotechnical engineering applications [1]. Distributed fiber optic sensing technology, as an effective method of SHM, has the advantages of long sensing distance, distributed sensing information and small sensor size [2]. In particular, Rayleigh and Brillouin based distributed fiber optic sensors have been developed to monitor distributed temperature and strain information for decades [3]–[5]. With the development of smart infrastructures, distributed dynamic measurement of strain can be used in more applications, such as detection of seismic activity, perimeter security and intrusion sensing, traffic monitoring, railway monitoring, and bridge monitoring [1], [6].

Phase-sensitive optical time domain reflectometry (phase-OTDR), the most studied Rayleigh based dynamic system, has been proved to be capable of detecting strain vibration as accurate as $0.08\mu\varepsilon$ [7]. However, it can only give relative strain between two strain conditions [8], [9]. In addition, phase-OTDR has a limited strain range of as low as $2~\mu\varepsilon$ [8], and its linearity between phase and strain is sensitive to the intrinsic phase of the fiber [7], [8].

B. Li, L. Luo, and Y. Yu are with the Department of Engineering, University of Cambridge, Cambridge CB2 1PZ, U.K. (e-mail: bl350@cam.ac.uk; ll432@cam.ac.uk; yy347@cam.ac.uk).

K. Soga is with the Department of Civil and Environmental Engineering, University of California at Berkeley, Berkeley, CA 94720 USA (e-mail: soga@berkeley.edu).

J. Yan is with the Electronics and Computer Science Department, University of Southampton, Southampton SO17 1BJ, U.K. (e-mail: j.yan@soton.ac.uk).

Brillouin based dynamic systems can measure the absolute strain with a large strain range higher than $10^4\mu\varepsilon$. Brillouin based systems demonstrate a slow sampling rate (tens of Hz to a few hundred Hz) and a limited sensing distance from tens of meters to a few hundred meters [10]–[12].

Brillouin optical time-domain reflectometry (BOTDR) has the advantage of single-end access compared with Brillouin optical time-domain analysis (BOTDA). This means that BOTDR can work even if the optic fiber cable is broken halfway. At the construction site, this advantage brings huge benefits for the sensor deployment and testing. However, BOTDR usually needs a large number of averaging due to the weak power of spontaneous Brillouin scattering (SpBS) and the conventional frequency scanning method [13]. Recently, Short-time Fourier transform (STFT) algorithm is replacing the frequency scanning in BOTDR [12], [14]. STFT can reduce the averaging times and realize the dynamic strain measurement [12], [14], whose performance is limited by the signal-to-noise ratio (SNR) that is usually low in BOTDR [13].

Stimulated Brillouin scattering (SBS) is usually avoided in BOTDR, which weakens the injected power along long fiber under test (FUT) (tens of km) and shortens the sensing distance. For many civil engineering applications, however, the sensing distance requirement is reduced to 1km (e.g. the monitoring of piles and buildings), greatly shorter than the achievable sensing distance of BOTDR [13].

The introduction of small gain SBS in BOTDR could improve the power of Brillouin scattering and SNR. The number of averaging then can be reduced and the speed of dynamic strain measurement can be increased as well. In this paper, a small gain SBS based STFT-BOTDR is proposed and tested for the dynamic strain and vibration measurement. The input power limits, frequency uncertainties for given pulse durations, fiber lengths, and number of averaging are calculated, limited by nonlinear effects.

II. POWER LIMITATIONS

The light power of the signal injected into an optic fiber is limited by some parameters. Power depletion can occur if the input power is over the threshold, especially for a distributed fiber optic sensing system [13].

The forward stimulated Raman scattering (SRS), modulation instability (MI), and SBS are dominant factors, which limit the input pulse power in BOTDR [15]. The input threshold for each of these effects is normally defined as the input power when the induced power by the effect is as large as the input power [15]–[17].
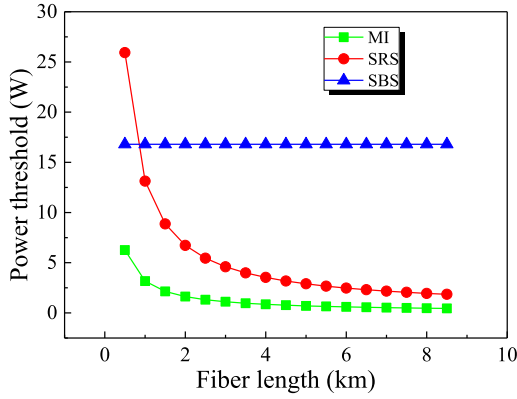
Fig. 1. MI, SBS and SRS thresholds at different fiber lengths with 40ns pulse duration ($g_R = 1 \times 10^{-13}$ m/W; $g_B = 2.5 \times 10^{-11}$ m/W; $\gamma = 1.78 W^{-1} km^{-1}$; $\beta_2 = -21.9$ps^2/km; $A_{eff} = 80 \times 10^{-12}$m^2).
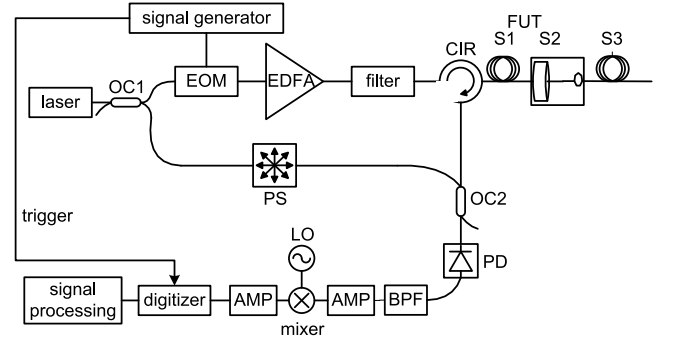

Fig. 2. Experimental setup for BOTDR (OC: optical coupler; EOM: electro-optic modulator; EDFA: erbium-doped fiber amplifier; CIR: circulator; PS: polarization scrambler: FUT: fiber under test; PD: photodetector; AMP: amplifier; LO: local oscillator; BPF: band pass filter).

The SRS input threshold P_{th-R} is given by [16]

$$P_{th-R} = \frac{16A_{eff}}{g_R L_{eff}} \tag{1}$$

where A_{eff} is the effective area of the fiber, g_R is the Raman gain coefficient, and L_{eff} is the fiber effective length.

MI can lead to the spectral sidebands symmetrically on both sides of the frequency of the incident light under the condition of anomalous group velocity dispersion, and the sidebands rise with the input power [17], [18].

The MI gain spectrumm is given by: [17]

$$g_{MI}(\omega) = |\beta_2 \omega| \left(\omega_c^2 - \omega^2 \right)^{1/2} \tag{2}$$

$$\omega_c^2 = \frac{4\gamma P_0}{|\beta_2|} \tag{3}$$

where β_2 is the fiber dispersion coefficient, P_0 is the input power, γ is the nonlinear parameter by SPM, ω is the frequency, and ω_c is the critical frequency below which MI gain exists.

The MI threshold P_{th-MI} is expressed as [15]

$$P_{th-MI} = \frac{11}{2\gamma L_{eff}} \tag{4}$$

The SBS threshold P_{th-B} is quantified by [17]

$$P_{th-B} = \frac{21A_{eff}}{g_B L} \tag{5}$$

where g_B is the Brillouin coefficient and L is the interaction length of Brillouin scattering, which equals to the spatial resolution of BOTDR.

When the interaction length of SBS is 4m at 40ns pulse duration, conventional SBS thresholds, MI thresholds and SRS thresholds at different fiber lengths are illustrated in Fig. 1. It shows that MI thresholds are smaller than SBS and SRS thresholds. In fact, by substituting the parameters with numerical values in (1) and (4) and using SI units, it can be derived that $P_{th-R} = 1.28 \times 10^4/L_{eff}$, $P_{th-MI} = 3.09 \times 10^3/L_{eff}$, $P_{th-B} = 67.2/L$. And hence

$$P_{th-R} = 4.14 P_{th-MI} \tag{6}$$

P_{th-R} is always larger than P_{th-MI}.

P_{th-MI} is only larger than P_{th-B} when $L_{eff}/L < 46$. For interaction length L of 4m, P_{th-B} becomes the dominant threshold when $L_{eff} < 184$m. However, under this condition, $P_{th-B} = 16.8$W, which is a high power for normal optic fiber and thermal effects might cause damage on the fiber.

Therefore for $L_{eff}/L \geq 46$, P_{th-MI} is the dominant threshold and determines the maximum input power for BOTDR.

III. ARCHITECTURE OF THE STFT-BOTDR

The BOTDR setup is schematically illustrated in Fig. 2. A narrow-linewidth external cavity laser provides continuous-wave (CW) light at 1550nm, followed by a 50/50 coupler (OC1) which splits the light into two branches. An electro-optic modulator (EOM) modulates one branch (the upper branch in Fig. 2) of the splitted light using a 40ns pulse at a repetition rate of 62.5kHz. The modulated light is amplified by a tunable erbium-doped fiber amplifier (EDFA). The output of the EDFA is filtered by a band pass filter (BPF) before being injected into a circulator. The FUT consists of a 920m standard single mode fiber (section S1) and a 15m single mode strain fiber (section S2 and section S3). fiber section S2 (about 6m long) is connected to a shaker which produces vibration on the fiber.

The lower branch of the signal from OC1 is an optical local oscillator (OLO), or the reference light, of the coherent detection system. A 700kHz polarization scrambler (PS) is added on this branch to provide random polarization and to reduce polarization fading noise. The reference light OLO and the Brillouin scattered light pass through another 50/50 coupler (OC2) and mix on a photodetector (PD). The PD output signal is downconverted by a 10.5GHz local oscillator, and is electronically filtered and amplified to produce the output signal. The output signal is captured by a digitizer at 5GSa/s and is processed on a computer by the STFT method.

Conventionally BOTDR systems use SpBS instead of SBS. For long sensing distances, SBS can cause large power depletion. For short fiber lengths (<1km for civil engineering applications), small SBS does not generate large power depletion and loose the constraint of the input pulse power threshold. Therefore, small gain SBS can be utilized in short sensing

fibers to enhance the SNR, which determines the detectability and accuracy of a BOTDR system [19]–[21]. The processing time can be reduced by SNR improvement and reduction of averaging times. The SNR calculation of the sensing system is given as [22]

$$
\begin{aligned}
SNR&(dB) \\
&= 10\log_{10}(\frac{2R^2 P_B P_{OLO}\sqrt{N}}{4kTB/R_L + 2eRP_{OLO}B + (RP_{OLO})^2 RINB}) \\
&\quad - NF_{E-noise}
\end{aligned}
\tag{7}
$$

where R is the responsivity of the photodetector, P_B is the Brillouin scattering power, P_{OLO} is the power of the local oscillator branch from the laser, N is the number of averaging, k is the Boltzmann constant, T is the temperature, B is the detected bandwidth, R_L is the load resistance, e is the electron charge, RIN is the relative intensity noise, and $NF_{E-noise}$ is the the the total noise figure of electronic components.

The power of the OLO branch is much higher than the Brillouin scattering signal. So the shot noise and the RIN noise (the second and the third terms of the denominator) can be approximated to be only related with P_{OLO}. Therefore, the thermal noise (the first term of the denominator), the shot noise and the RIN noise are independent of the Brillouin scattering power. Furthermore, for the BOTDR setup in this study, a total calculated electronic noise figure (NF) of 2.11dB is added onto the system, which is independent of the Brillouin power as well. The filtered noise by the EDFA seen on the PD can be neglected, as it is much smaller than the shot noise and thermal noise. Hence, the SNR is mainly influenced by the numerator. With the same setup, the increase of the Brillouin scattering power can enhance the numerator of (7) and the SNR.

IV. CALCULATION OF THE SYSTEM PERFORMANCE

SpBS is a linear process. The Stokes and anti-Stokes signals are located symmetrically on both sides of the Rayleigh signal on the optical spectrum with similar power for the SpBS. The SpBS power P_{SpBS} induced in an optic fiber can be calculated as [8]:

$$
P_{SpBS} = T_{pulse} S \gamma_{SpBS} P_0
\tag{8}
$$

where T_{pulse} is the pulse duration, S is the capture fraction, and γ_{SpBS} is the SpBS coefficient.

SBS occurs as the input peak pulse power increases. The SBS is a nonlinear process, whose Stokes signal power is exponentially amplified by increased input power. The Brillouin single-pass gain G_B of SBS is expressed as [23]

$$
G_B = \frac{g_B P_0 L}{A_{eff}}
\tag{9}
$$

Considering the pulse duration adopted in BOTDR, the SBS induced Stokes power by SBS generator on optic fiber can be calculated as [23]

$$
P_B = \begin{cases} P_N e^{G_B} & \Gamma_B T_{pulse} > G_B/2 \\ P_N e^{-2\Gamma_B T_{pulse} + 2\sqrt{2G_B \Gamma_B T_{pulse}}} & \Gamma_B T_{pulse} < G_B/2 \end{cases}
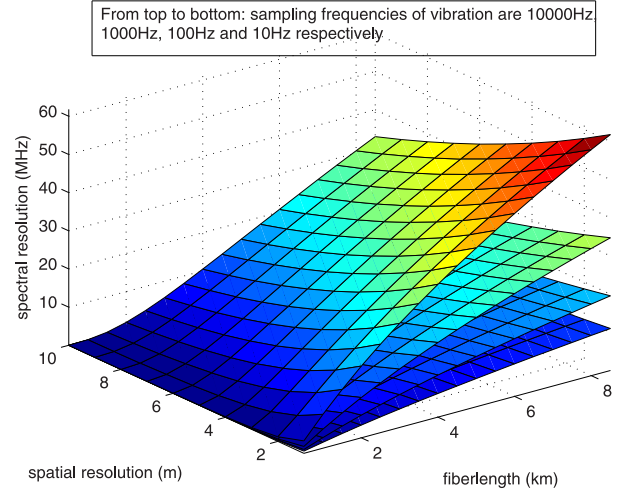\tag{10}
$$

Fig. 3. Calculation of BFS uncertainty at different fiber lengths, spatial resolution and sampling frequency.

where P_N is the noise that initiates the SBS process and Γ_B is the phonon damping rate. P_N is usually calculated as a fixed fraction of the injected light power [17]. A typical phonon lifetime $1/\Gamma_B$ of optic fiber is 5ns [17].

As is derived in (7), the Brillouin power is a main factor that influences SNR. The detected spectral resolution ($\delta\nu_B$) of BOTDR is related with SNR, the frequency step (σ) and the Brillouin bandwidth ($\Delta\nu_B$) as given by [24]:

$$
\delta\nu_B = 0.67 \times \sqrt{\frac{\sigma \cdot \Delta\nu_B}{SNR}}
\tag{11}
$$

Hence, a higher SNR leads to a better spectral resolution for the system.

The Brillouin bandwidth is typically about 30MHz (as a function of phonon damping factor) for SpBS and small gain SBS. It becomes narrower with larger Brillouin gain. For the FUT used, the Brillouin bandwidth is about 60MHz.

The dynamic sampling rate of BOTDR is given by

$$
f_{samp} = \frac{1}{T_0 N}
\tag{12}
$$

where T_0 is the period of the input pulse and N is the averaging number. T_0 is set to be larger than the total time (T_{period}) needed for the pulse to travel into and back from the FUT to eliminate overlap. The shortest time T_0 is given by

$$
T_0 = T_{period} = \frac{2L_0}{v_g}
\tag{13}
$$

where L_0 is the fiber length and v_g is the group velocity of light.

Using (7) and (9)-(13), the uncertainty of Brillouin frequency shift (BFS) can be theoretically modelled. Using (4), the MI threshold, i.e. the maximum input pulse power at a given fiber length, can be calculated. Consequently, the best BFS uncertainty at a given spatial resolution, fiber length and sampling frequency can be derived, as shown in Fig. 3. It shows a good spectral resolution with a fiber length below 2km.
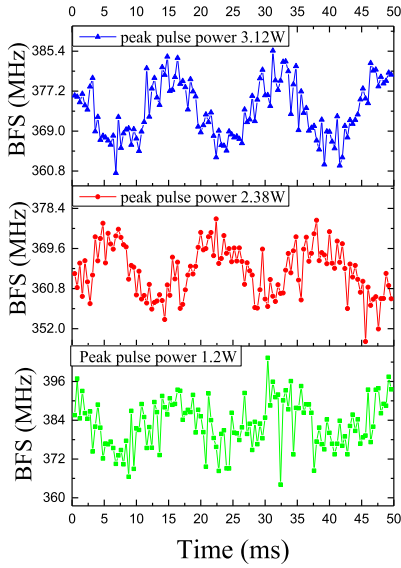
Fig. 4. Measured 60Hz strain vibration at different input peak pulse power levels.

V. EXPERIMENTAL RESULTS OF DYNAMIC STRAIN SENSING

The dynamic strain measurement by BOTDR is experimentally verified with 60Hz vibration frequency on a shaker. The EDFA output power is tuned to produce different injected peak pulse power into FUT, at 1.2W, 2.38W and 3.12 W, respectively.

The input pulse is 40ns wide with $16\mu s$ period (62.5 kHz repetition frequency), leading to 4m spatial resolution. The output signal is captured by a digitizer for 50ms each measurement and is processed with an averaging number of 25 to derive each profile of BFS, leading to 2.5kHz sampling rate for vibration detection. According to Nyquist principle, a vibration at up to 1.25 kHz can be detected. By setting a faster pulse repetition frequency, the vibration sampling rate can be faster and reach up to 4kHz for 1km fiber under the condition of 100kHz pulse repetition for $10\mu s$ period. The spatial sampling resolution is set to 0.4m by setting the step of STFT, which means that there is a BFS result along the fiber in every 0.4m.

The measured strain vibration over 50ms is shown in Fig. 4, by averaging the derived BFS over fiber section S2. At 3.12W input peak pulse power, a clear sine waveform can be identified. The measured peak-to-peak change of BFS is about 16MHz, corresponding to 320 $\mu\varepsilon$ strain change on the fiber. At 1.2W peak pulse power, the shape of the derived waveform is much more distorted. Via sine fitting, the R-square values of 0.75, 0.59 and 0.37 are derived for the peak pulse power of 3.12W, 2.38W and 1.2W, respectively. Spectra of these measured strain vibration profiles in Fig. 4 are demonstrated in Fig. 5. A frequency component at 60Hz can be seen in Fig. 5 for each input power level. Furthermore, the noise level at 1.2W is the highest among the three spectra while the spectra at 3.12W gives the lowest noise level. The experimental result at 3.12W with SBS effect gives a better detection of strain vibration at 2.5kHz sampling rate.
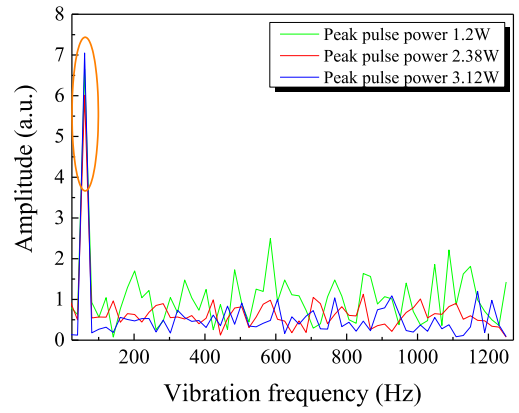

Fig. 5. Spectra of the measured strain vibration profiles by Fourier transform.
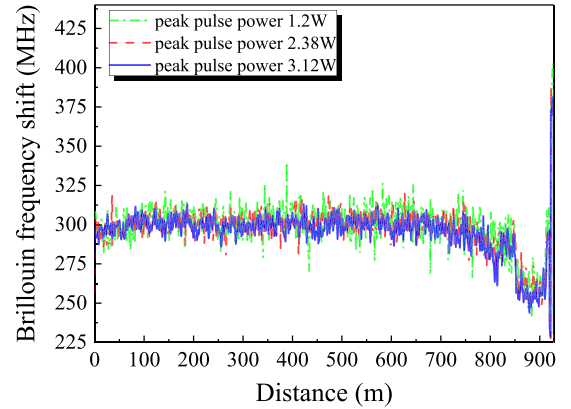

Fig. 6. Measured profiles of Brillouin frequency shift (BFS) at different input peak pulse power.

The corresponding profiles of BFS obtained after signal processing are illustrated in Fig. 6. From 850m to 910m, the BFS drops for about 40 MHz due to the initial condition of the fiber. The fluctuation of the measured BFS at peak pulse power of 1.2W is much larger than that at 3.12W. The corresponding frequency uncertainty for each input power level is calculated as the standard deviation of the measured BFS over time. The uncertainties are 5.1MHz, 6.3MHz, and 10.7MHz at 3.12W, 2.38W and 1.2W input peak pulse power, respectively. Fig. 7 shows the measured frequency uncertainties compared by the estimated frequency uncertainties using (7) and (9)-(13).

The vibration of strain is added onto fiber section S2 with about 150MHz ($3000\mu\varepsilon$) pre-strain. The BFS profiles of S2 are enlarged in Fig. 8 (a). The difference in BFS amplitudes among different input levels is caused by the strain vibration. In Fig. 8 (a), the rising edge of BFS for the input peak pulse power of 3.12W is from 922m to 922.4m. The rising edge of detected BFS profile for the case of 2.38W peak pulse power is one sampling point (0.4m) later than that for the case of 3.12W. The rising edge for the case of 1.2W peak pulse power is further delayed. This is the distance error in time domain due to the double-peak effect of the BFS spectra in frequency domain with large BFS change [14]. With a worse SNR in the case of 1.2W, compared with that for the other two profiles, the distance error is more obvious due to the amplitude error of detected BFS by small SNR and the double-peak effect.
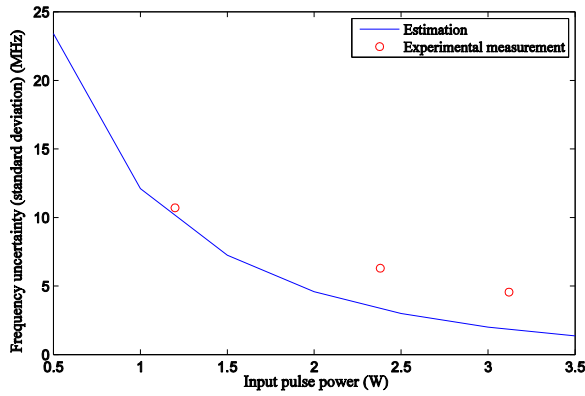
Fig. 7. Frequency uncertainty (standard deviation) by experimental measurement compared with estimation.

The BFS power profiles corresponding to each BFS profile in Fig. 8 (a) is given in Fig. 8 (b). The points in the orange rectangle are the detected Brillouin power of the sampling points on the rising edges of the BFS profiles in Fig. 8 (a). In the cases of 3.12W and 2.38W, a local minimum point can be found in the rectangular in Fig. 8 (b). At this transition point, the double peak effect splits the detected Brillouin power onto two BFS. Hence, the detected power of a single BFS drops. The spectra of the sampling points on the rising edges in Fig. 8 (a) are drawn in Fig. 8 (c). It can be seen in Fig. 8 (c) that the larger the peak pulse power is, the better the SNR is. The distance error effect can be smaller as well accordingly.

The static performance of BOTDR is measured with the shaker off.

With the same settings, the power traces of measured BFS along the FUT at different input power levels are obtained with 25 times of averaging, as shown in Fig. 9. At the input levels below 3.51W, the power attenuation is very small and can be negligible at 1.2W. In the case of 3.51W, the power depletion caused by MI can be clearly observed and it cuts down the SNR at the far end of FUT. This power level (3.51 W) can be seen as the MI threshold for this fiber length [15]. The inset inside Fig. 9 is the measured optical spectra at the far end of the FUT in the cases of 2W, 3.12W and 3.52W, respectively. In the case of 2W, no MI is observed on the spectrum. In the case of 3.12W, a small MI can be seen located on both sides of the signal frequency. This MI spectrum grows significantly when peak pulse power increases to 3.52W. By integrating the MI spectrum, the MI power is 10dB lower than the signal power in the case of 3.12W, whereas the integrated MI power equals to the signal power in the case of 3.52W, which reaches the MI threshold.

The measured Brillouin Stokes and anti-Stokes power, and the calculated SpBS power and SBS power by (8) and (10) are shown in Fig. 10. The measured Stokes power increases much faster than the anti-Stokes power and shows an exponential growth as the input peak pulse power rises. The measured Stokes power matches the calculated SBS power. The measured anti-Stokes power shows a good fit with the calculated SpBS power. As discussed by Boyd [23], the anti-Stokes SBS
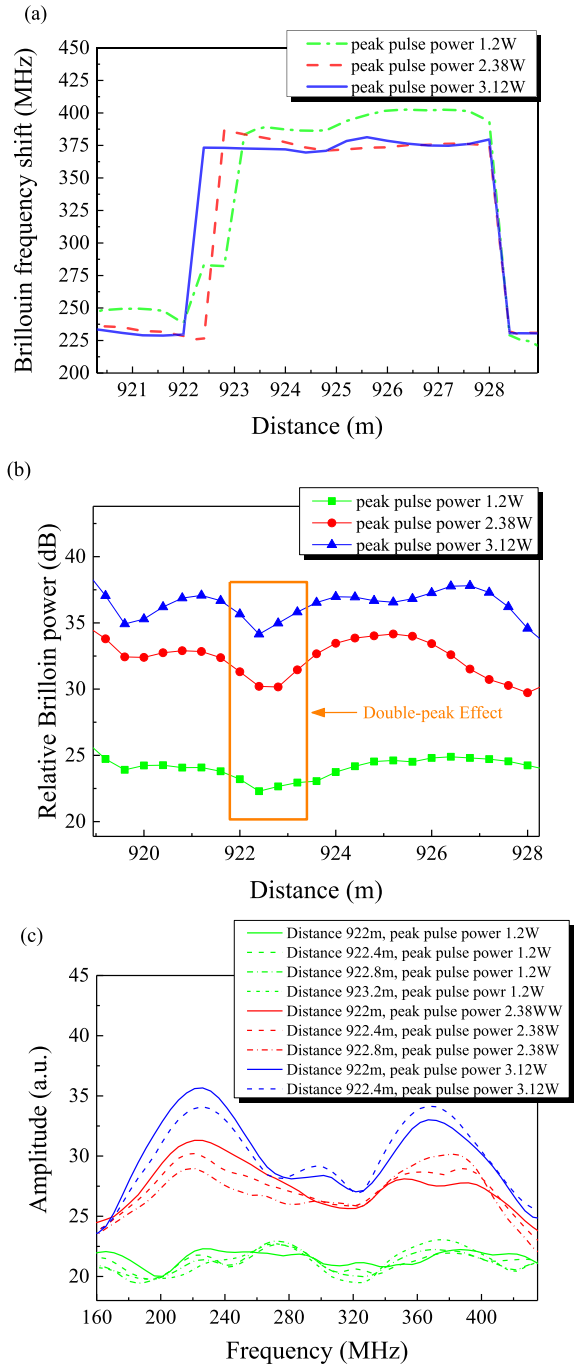

Fig. 8. (a) Measured BFS profiles on fiber section S2. (b) Power profiles for BFS at different input peak pulse power. (c) Spectra at each sampling point of the rising edges in (a).

propagates in positive direction along the fiber and attenuates exponentially. Hence the measured anti-Stokes can be seen as SpBS. Around 1.1W, SBS and SpBS have the same power and SBS becomes dominant as the input peak pulse power continues rising. 1.2W is used as the threshold for small gain SBS in experiment, as demonstrated in Fig. 4. Apparently, even at the input peak pulse power of 4.19W, the SBS power is still below the conventional SBS threshold which is mostly defined to be 100% or 1% of input power. But small gain SBS can be clearly seen under this condition from Fig. 10.
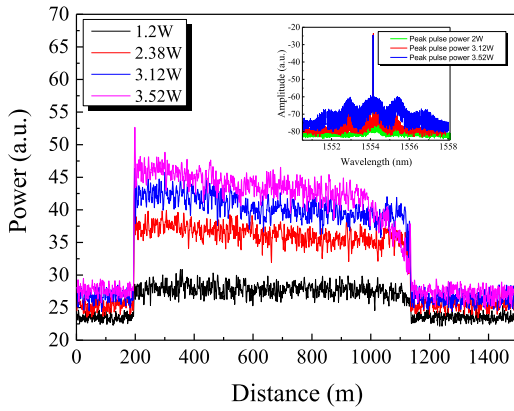
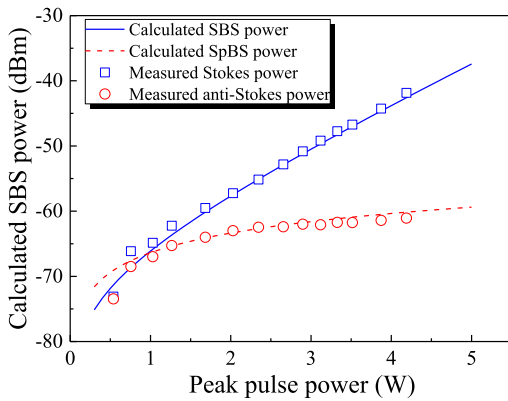Fig. 9.   Power traces of BFS at different input power and the measured optical spectra at different power.

Fig. 10.   Measured Stokes and anti-Stokes power of Brillouin scattering at different input peak pulse power and calculated SBS and SpBS power.

VI. CONCLUSION

The input peak pulse power thresholds at short sensing distance are calculated. At sensing distance within 1km, peak pulse power can be raised up compared with long sensing distance. Small gain SBS is used in BOTDR system to enhance SNR and to achieve fast dynamic strain detection. A small gain SBS based BOTDR system of distributed dynamic strain vibration measurement is established with the capacity to measure as high as 1.25 kHz vibration. A vibration of 60Hz on a fiber section of 6 meters is successfully detected.

REFERENCES

[1] B. Shi, H. A. Sui, J. Liu, and D. Zhang, "The BOTDR-based distributed monitoring system for slope engineering," in *Proc. IAE*, vol. 683, 2006, pp. 1–5.

[2] J. Geng, S. Staines, M. Blake, and S. Jiang, "Distributed fiber temperature and strain sensor using coherent radio-frequency detection of spontaneous Brillouin scattering," *Appl. Opt.*, vol. 46, no. 23, pp. 5928–5932, 2007.

[3] T. Horiguchi, K. Shimizu, T. Kurashima, M. Tateda, and Y. Koyamada, "Development of a distributed sensing technique using Brillouin scattering," *J. Ligthw. Technol.*, vol. 13, no. 7, pp. 1296–1302, Jul. 1995.

[4] Y. Mizuno, W. Zou, Z. He, and K. Hotate, "Proposal of Brillouin optical correlation-domain reflectometry (BOCDR)," *Opt. Exp.*, vol. 16, no. 16, pp. 12148–12153, 2008.

[5] X. Bao and L. Chen, "Recent progress in optical fiber sensors based on Brillouin scattering at University of Ottawa," *Photon. Sensors*, vol. 1, no. 2, pp. 102–117, 2011.

[6] R. Bernini, A. Minardo, and L. Zeni, "Dynamic strain measurement in optical fibers by stimulated Brillouin scattering," *Opt. Lett.*, vol. 34, no. 17, pp. 2613–2615, 2009.

[7] A. Masoudi, M. Belal, and T. P. Newson, "A distributed optical fibre dynamic strain sensor based on phase-OTDR," *Meas. Sci. Technol.*, vol. 24, no. 8, p. 85204, 2013.

[8] A. Masoudi and T. P. Newson, "Contributed review: Distributed optical fibre dynamic strain sensing," *Rev. Sci. Instrum.*, vol. 87, no. 1, p. 11501, 2016.

[9] A. Masoudi, M. Belal, and T. P. Newson, "Distributed dynamic large strain optical fiber sensor based on the detection of spontaneous Brillouin scattering," *Opt. Lett.*, vol. 38, no. 17, pp. 3312–3315, 2013.

[10] Y. Peled, A. Motil, L. Yaron, and M. Tur, "Slope-assisted fast distributed sensing in optical fibers with arbitrary Brillouin profile," *Opt. Exp.*, vol. 19, no. 21, pp. 19845–19854, 2011.

[11] K. Y. Song, M. Kishi, Z. He, and K. Hotate, "High-repetition-rate distributed Brillouin sensor based on optical correlation-domain analysis with differential frequency modulation," *Opt. Lett.*, vol. 36, no. 11, pp. 2062–2064, 2011.

[12] G. Tu, X. Zhang, Y. Zhang, Z. Ying, and L. Lv, "Strain variation measurement with short-time Fourier transform-based Brillouin optical time-domain reflectometry sensing system," *Electron. Lett.*, vol. 50, no. 22, pp. 1624–1626, 2014.

[13] X. Bao and L. Chen, "Recent progress in Brillouin scattering based fiber sensors," *Sensors*, vol. 11, no. 4, pp. 4152–4187, 2011.

[14] Y. Yu, L. Luo, B. Li, L. Guo, J. Yan, and K. Soga, "Double peak-induced distance error in short-time-Fourier-transform-Brillouin optical time domain reflectometers event detection and the recovery method," *Appl. Opt.*, vol. 54, no. 28, pp. E196–E202, 2015.

[15] S. M. Foaleng and L. Thévenaz, "Impact of Raman scattering and modulation instability on the performances of Brillouin sensors," *Proc. SPIE 7753, 21st Int. Conf. Opt. Fiber Sens.*, 77539V, May 17, 2011, doi: 10.1117/12.885105.

[16] R. G. Smith, "Optical power handling capacity of low loss optical fibers as determined by stimulated Raman and Brillouin scattering," *Appl. Opt.*, vol. 11, no. 11, pp. 2489–2494, Nov. 1972.

[17] G. Agrawal, *Nonlinear Fiber Optics*, 5th ed. Oxford, U.K.: Academic, 2013.

[18] M. N. Alahbabi, Y. T. Cho, T. P. Newson, P. C. Wait, and A. H. Hartog, "Influence of modulation instability on distributed optical fiber sensors based on spontaneous Brillouin scattering," *J. Opt. Soc. Amer. B, Opt. Phys.*, vol. 21, no. 6, pp. 1156–1160, 2004.

[19] L. Thévenaz and M. A. Soto, "Rating the performance of a Brillouin distributed fiber sensor," *Proc. SPIE 8421, OFS2012 22nd Int. Conf. Opt. Fiber Sens.*, 8421A7, Oct. 4, 2012, doi: 10.1117/12.975290.

[20] L. Thévenaz and M. A. Soto, "Brillouin distributed fiber sensors: Practical limitations and guidelines for the making of a good sensor," in *Proc. IEEE Sensors*, Nov. 2014, pp. 146–149.

[21] M. A. Soto and L. Thévenaz, "Modeling and evaluating the performance of Brillouin distributed optical fiber sensors," *Opt. Exp.*, vol. 21, no. 25, pp. 31347–31366, 2013.

[22] Y. Lu, Y. Yao, X. Zhao, F. Wang, and X. Zhang, "Influence of non-perfect extinction ratio of electro-optic modulator on signal-to-noise ratio of BOTDR," *Opt. Commun.*, vol. 297, pp. 48–54, Jun. 2013.

[23] R. W. Boyd, *Nonlinear Optics*, 3rd ed. Burlington, MA, USA: Academic, 2008.

[24] Y. Yu, L. Luo, B. Li, K. Soga, and J. Yan, "Frequency resolution quantification of Brillouin-distributed optical fiber sensors," *IEEE Photon. Technol. Lett.*, vol. 28, no. 21, pp. 2367–2370, Nov. 1, 2016, doi: 10.1109/LPT.2016.2594084.
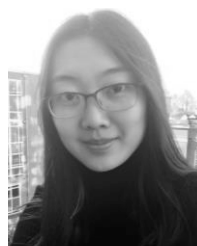
Bo Li received the B.Eng. (Hons.) degree in communication systems engineering from the University of Birmingham, U.K., the B.Eng. degree in communication engineering from the Harbin Institute of Technology in 2012, and the M.Res. degree in photonic systems development from the University of Cambridge, U.K., in 2013. She is currently pursuing the Ph.D. degree with the Cambridge Center of Smart Infrastructure and Construction. Her current research interests include the dynamic measurement of Brillouin scattering-based distributed fiber optic sensing technology. She is a member of Wolfson College with the University of Cambridge.

Linqing Luo received the B.Eng. (Hons.) degree in electrical engineering from the University of Liverpool, the B.Eng. degree in electrical engineering and automation from Xi'an Jiaotong Liverpool University, in 2012, and the M.Res. degree in photonic systems development from the University of Cambridge in 2013. He is currently pursuing the Ph.D. degree with the Cambridge Center of Smart Infrastructure and Construction, Hughes Hall of the University of Cambridge in 2013. His current research interests include Brillouin-based distributed fiber optic sensing system.

Kenichi Soga received the B.Eng. and M.Eng. degrees in civil engineering from Kyoto University, in 1987 and 1989, respectively, and the Ph.D. degree in civil engineering from the University of California at Berkeley, Berkeley, CA, USA.

He is Chancellor's Professor with the University of California at Berkeley, and formerly Professor of Civil Engineering with the University of Cambridge. He has published more than 350 journal and conference papers. His current activities interests include innovative monitoring and long-term performance of civil engineering infrastructure, energy geomechanics, and modeling of underground construction processes. He is Fellow of the Royal Academy of Engineering and the Institution of Civil Engineers. He is a founding member of the Cambridge Centre for Smart Infrastructure and Construction and has led the sensor and data analysis group prior to his move to Berkeley. He is a recipient of many awards, including the George Stephenson Medal and the Telford Gold Medal from the Institution of Civil Engineers and the Walter L. Huber Civil Engineering Research Prize from the American Society of Civil Engineers.

Yifei Yu received the bachelor's (Hons.) degree in electronics and communications engineering with the University of Bristol in 2011, and the M.Phil. degree in MEMS from the Nanoscience Center, University of Cambridge, where she is currently pursuing the Ph.D. degree with the Geotechnical and Environmental Engineering Research Group. Her current research interests include the signal processing of Brillouin scattering-based fiber optics sensing. She is a member of Newnham College, University of Cambridge.

Jize Yan received the degree from Tsinghua University, China, and the Ph.D. degree from the University of Cambridge.

He is an Associate Professor of Electronics and Computer Science with the University of Southampton. His research work has resulted in 80+ peer-reviewed publications, nine patents, and a number of best paper awards. His research interests include microsystems (optomechanics, MEMS) and sensor systems. He has co-founded two companies in the field of wireless sensor network and energy harvesting to develop industrial applications. He is a member of the Southampton Nanofabrication Centre, Zepler Institute, and the Centre for Risk Research, University of Southampton.